

Learnt dynamics generalizes across tasks, datasets, and populations

U. Mahmood¹, M. M. Rahman¹, A. Fedorov², Z. Fu¹, V. D. Calhoun^{1,2,3}, S. M. Plis¹
 Tri-institutional Center for Translational Research in Neuroimaging and Data Science:
¹Georgia State University, ²Georgia Institute of Technology, ³Emory University
 Atlanta, GA, USA

{umahmood1, mrahman21}@student.gsu.edu afedorov@gatech.edu
 {zfu, vcalhoun, splis}@gsu.edu

Abstract

Differentiating multivariate dynamic signals is a difficult learning problem as the feature space may be large yet often only a few training examples are available. Traditional approaches to this problem either proceed from handcrafted features or require large datasets to combat the $m \gg n$ problem. In this paper, we show that the source of the problem—signal dynamics—can be used to our advantage and noticeably improve classification performance on a range of discrimination tasks when training data is scarce. We demonstrate that self-supervised pre-training guided by signal dynamics produces embedding that generalizes across tasks, datasets, data collection sites, and data distributions. We perform an extensive evaluation of this approach on a range of tasks including simulated data, keyword detection problem, and a range of functional neuroimaging data, where we show that a single embedding learnt on healthy subjects generalizes across a number of disorders, age groups, and datasets.

1. Introduction

Many interesting domains and systems are best characterized by their multivariate dynamics. Short and long term weather fluctuations, speech and ambient sound, and, importantly, function of human brain to name a few. Often in these applications we need to differentiate one condition from another based on these dynamics. Although handcrafting features for a classifier is a common and widespread approach, discarding potentially valuable information, when we know that dynamics is the key to the system’s behavior, is suboptimal. Especially when one of the goals is to learn what determines a condition of the system.

Consider a simple problem of training devices to recognize custom keywords with minimal training. This is a setting where only a few training samples can be expected.

Arguably more important domain to deal with is the area of mental health.

Mental disorders manifest in behavior that is driven by disruptions in brain dynamics [1, 2]. Functional MRI captures the nuances of spatio-temporal dynamics that could potentially provide clues to the causes of mental disorders and enable early diagnosis. However, the obtained data for a single subject is of high dimensionality m and to be useful for learning, and statistical analysis, one needs to collect datasets with a large number of subjects n . Yet, for any kind of a disorder, demographics or other types of conditions, a single study is rarely able to amass datasets large enough to go out of the $m \gg n$ mode. Traditionally this is approached by handcrafting features [3] of much smaller dimension, effectively reducing m via dimensionality reduction. Often, the dynamics of brain function in these representations vanishes into proxy features such as correlation matrices of functional network connectivity (FNC) [4]. Efforts that pull together data from various studies and increase n do exist, but it is difficult to generalize to study of smaller and more specific disease populations that cannot be shared to become a part of these pools or are too different from the data in them.

Our goal is to enable the direct study of systems dynamics in smaller datasets. In the case of brain data it, in turn, can enable an analysis of brain function. In this paper, we show how one can achieve significant improvement in classification directly from dynamical data on small datasets by taking advantage of publicly available large but unrelated datasets. We demonstrate that it is possible to train a model in a self-supervised manner on dynamics of healthy control subjects from the Human Connectome Project (HCP) [5] and apply the pre-trained encoder to a completely different data collected across multiple sites from healthy controls and patients. We show that pre-training on dynamics allows the encoder to generalize across a number of datasets and a wide range of disorders: schizophrenia, autism, and Alzheimer’s disease. Importantly, we show that learnt dy-

namics generalizes across different data distributions, as our model pre-trained on healthy adults shows improvements in children and elderly. The generality of the approach is also demonstrated in an application to the keyword detection problem.

2. Related Work

Unsupervised pre-training is a well-known technique to get a head start for the deep neural network. It may be considered as a regularizer which compares to classical regularizers (i.e. L1/L2) may not vanish even with more data and could find a robust local minima for better generalization [6]. Classical methods are Deep Beliefs Networks (DBMs) [7] and stacked denoising autoencoders (SDAE) [8]. Unsupervised pre-training has broad implications in fields such as computer vision [9], natural language processing (NLP) (GPT2 [10], BERT [11], Word2Vec [12]) and automatic speech recognition (ASR) (with SDAE [13], with DBN-HMMs [14]). However, this unsupervised pre-training is considered to be less popular in fields other than NLP [15]. Specifically, in computer vision, researchers usually use the model which is pre-trained in supervised fashion on Imagenet as a starting point for downstream tasks. Furthermore, given enough data and technical strategies, it is possible to achieve better results on COCO object detection without supervised pre-training on Imagenet [16].

Recent advances in unsupervised learning using self-supervised methods with mutual information objectives have reduced the gap between supervised and unsupervised learning on standard computer vision classification datasets [17–21] and scaled pre-training to very deep convolutional networks (e.g., 50-layer ResNet). Furthermore, it influences the neuroimaging field for classification of progression to Alzheimer’s disease from sMRI [22], learning useful representation of the states from the frames in Atari games [23] and also from the speech chunks for speaker identification [24]. Specifically, authors [19] have shown that contrastive based self-supervised pre-training can outperform supervised methods by a large margin in case of small data (e.g., 13 images per class in ImageNet [25]).

In most cases, due to practical reasons, researchers in brain imaging are constrained to work with small datasets. In addition, earlier work [26, 27] in brain imaging have been based on unsupervised methods to learn the dynamics and structure of the brain while supervised approaches are used to perform predictions at individual level. Such unsupervised methods include models as linear ICA [28], HMM framework [29]. Moreover, some other nonlinear approaches are also proposed to capture the dynamics. Examples include using Restricted Boltzman Machines (RBMs) [30], RNN modification of ICA [31], and reconstructions by recurrent U-Net architecture [32]. In some cases, where dataset is very small, transfer learning as observed in some neuroimaging

application [33–35] is considered as a way to enable learning from data and thus improve results in downstream classification. To achieve improved performance, another idea is the data generating approach [36] which uses synthetic data generator for pre-training, relieving the scarcity of data.

3. Methods

Our method is two fold. We first pre-train our encoder on large unrelated dataset to learn improved representation of the latent factors, and then use the pre-trained encoder for downstream task. We explain both steps in the following sections.

3.1. Pre-training

3.1.1 Spatio-Temporal DeepInfoMax

For self-supervised pre-training we use Spatio-Temporal DeepInfoMax [23] to maximize predictability between current latent state and future spatial state and between consecutive spatial states (for example, on encoded time points of the resting-state fMRI (rsfMRI)).

Let $D = \{(u_t, v_s) : 1 \leq t, s \leq N, t \neq s\}$ be a dataset of pairs of values at time point t and s sampled from sequence with length N . Then $D^+ = \{(u_t, v_s) : 1 \leq t \leq N - 1, s = t + 1\}$ is called a dataset of positive pairs and $D^- = \{(u_t, v_s) : 1 \leq t, s \leq N, s \neq t + 1\}$ — of negative pairs. The dataset D^+ refers to a joint distribution and D^- — a marginal distribution. Eventually, the lower bound with InfoNCE estimator [37] $\mathcal{I}_f(D^+)$ is defined as:

$$\mathcal{I}(D^+) \geq \mathcal{I}_f(D^+) \triangleq \sum_{t=1}^N \log \frac{\exp f((u_t, v_{t+1})^+)}{\sum_{s=1}^N \exp f((u_t, v_s)^-)}, \quad (1)$$

where f is a critic function [38]. Specifically, we are using separable critic $f(u_t, v_s) = \phi(u_t)^\top \psi(v_s)$, where ϕ and ψ are some embedding functions parameterized by neural networks. Such embedding functions are used to calculate value of a critic function in same dimensional space from two dimensional inputs. Critic learns an embedding function such that critic assigns higher values for positive pairs compared to negative pairs: $f(D^+) \gg f(D^-)$.

We define a latent state as an output z_t of encoder E and a spatial state c_t^l as the output of l th layer of the encoder for input x_t at time point t . To optimize the objective between current latent state and future spatial state, the critic function for input pair (x_t, x_s) is $f_{global} = \phi(z_t)^\top \psi(c_s^l)$ and between consecutive spatial states — $f_{local} = \psi(c_t^l)^\top \psi(c_s^l)$. Finally, the loss is the sum of the InfoNCE with f_{global} and InfoNCE with f_{local} as $L = I_{f_{global}} + I_{f_{local}}$. The scheme of the ST-DIM is shown in Figure 1.

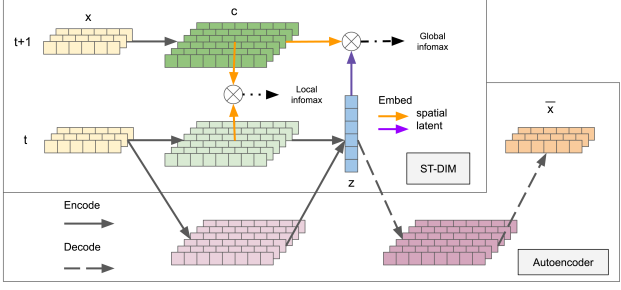


Figure 1. Spatio-Temporal Deep InfoMax (ST-DIM) and autoencoder architecture used in pre-training. To enable comparison, the same encoder architecture is used for both ST-DIM and autoencoder models.

3.1.2 Autoencoder

An autoencoder [39] is often viewed as an unsupervised learning representation technique useful for obtaining an informative representation of the input for downstream tasks [15]. As implied in its name, it consists of two phases, namely, reduction (encoding) and reconstruction (decoding). In the reduction phase, the autoencoder compresses its input preserving useful latent representation of the input. In the reconstruction phase, it learns to create outputs similar to inputs based on the latent representation achieved in reduction phase. Both phases are trained together to obtain optimal results. The reduction and reconstruction phases can be considered as two mathematical functions $\Phi : \mathcal{X} \mapsto \mathcal{F}$ and $\Psi : \mathcal{F} \mapsto \mathcal{X}$ respectively. We use the mean-squared error for the loss function which is defined as: $\mathcal{L}(x, \hat{x}) = \|x - \hat{x}\|^2 = \|x - \Psi(\Phi(x))\|^2$, where $x, \hat{x} \in \mathcal{X}$ and refer to input and output of the autoencoder respectively. Though autoencoder can be implemented using different types of networks, we use the same network architecture as used for ST-DIM pre-training (See Section 4.1) to make them ideally comparable. The architecture used in pre-training is shown in Figure 1.

3.2. Transfer and Supervised Learning

In the downstream task, we use the representation of the encoder pre-trained using ST-DIM or autoencoder as input to a biLSTM [40] and add a simple binary classifier on top. We also use the same encoder architecture to learn end-to-end supervised model (i.e., no pre-trained weights) for the same classification tasks. The overall architecture used for downstream tasks is shown in Figure 2. Refer to section 4.1 for further details.

4. Experiments

In this section we study the performance of our model on both, synthetic and real data. To compare and show the advantage of pre-training on large unrelated dataset we use three different kind of models — 1) FPT (Frozen Pre-

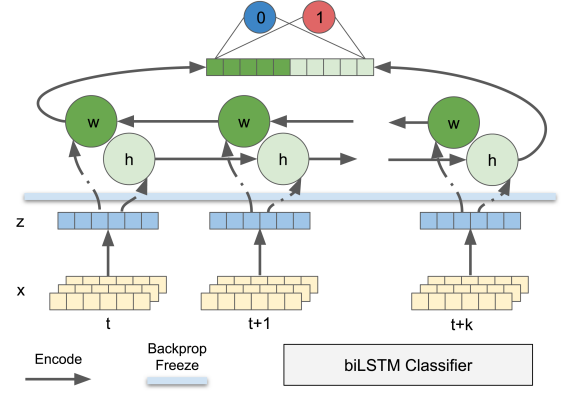


Figure 2. Architecture used in downstream task. Windows (time slices) are encoded using encoder described in Section 3.1.2 and passed through a biLSTM. Outputs of the last forward and backward LSTM layers are concatenated and passed through a dense layer for classification.

Trained): The pre-trained encoder is not further trained on the dataset of downstream task, 2) UFPT (Unfrozen Pre-Trained): The pre-trained encoder is further trained on the dataset of downstream task and 3) NPT (Not Pre-trained): The encoder is not pre-trained at all and only trained on the small dataset of downstream task. The models are shown in Figure 3. In each experiment, we compare all three models to demonstrate the effectiveness of unsupervised pre-training.

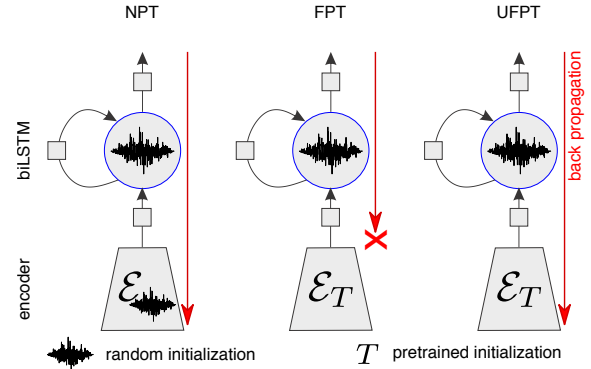


Figure 3. Three different models are used for downstream tasks: 1) In FPT, we pre-train our encoder but keep it frozen during downstream task. 2) In UFPT, we pre-train our encoder but continue training during downstream task. 3) In NPT, we use the exactly same architecture but with no pre-trained weights for the encoder.

4.1. Setup

Encoder for simulation experiment consists of 4 1D convolutional layers with output features (32, 64, 128, 64), kernel sizes (4, 4, 3, 2) respectively, followed by ReLU [41] after each layer followed by a linear layer with 256 units. For real data experiments, we use 3 1D convolutional layers with output features (64, 128, 200), kernel sizes (4, 4, 3) re-

spectively, followed by ReLU after each layer followed by a linear layer with 256 units. We use stride 1 for all of the convolution layers. For the autoencoder based pre-training for simulation experiment, we use the same encoder as for ST-DIM in the reduction phase. For the decoder, we use the reverse architecture of the encoder. Precisely, we use a linear layer with 704 units followed by 4 1D transpose convolution layers with output features (128, 64, 32, 10), kernel sizes (2, 3, 4, 4) respectively and all with stride 1, that result in 10×20 windows at the output.

In ST-DIM based pre-training, for all possible pairs in the batch, we take features c^3 and z after the 3rd convolutional layer and output layer respectively. We embed both c^3 and z using ψ and ϕ respectively to a 128 dimensional vector to compute the score of a critic function f_{global} or f_{local} . Using these scores, we compute the loss. The neural networks are trained using Adam optimizer [42]. The weights for encoder are initialized using orthogonal initialization. However, the LSTM and the final fully connected layer are initialized using Xavier [43].

As we are more interested in subjects for classification task, we feed each time series (ICA time courses) into the encoder in the form of a sequence of windows. The encoder encodes the windows of input data into latent representation. The latent representation of the entire time series is then concatenated and passed to a biLSTM with hidden dimension of size 200. The output of biLSTM is then used as input to a feed forward network of two linear layers with 200 and 2 units to perform binary classification.

For experiments on the downstream tasks, a hold out is selected for testing and is never used through the training/validation phase. For each downstream task, the number of subjects used for supervised training is gradually increased within a range to observe the effectiveness of pre-training in downstream task with varied number of training subjects. For each experiment, 10 trials are performed to ensure random selection of training subjects and, in each case, the performance is evaluated on the hold out dataset (test data).

For brain data, each of the models (FPT, UFPT, NPT) yields the best results based on its respective gain value of Xavier [43] initialization used for biLSTM. To find the best gain value for each model, 20 values in the range 0 – 1 are tried with an increment of 0.05. For each value, 10 experiments are performed and best value is chosen based on the results on validation dataset. Refer to Table 1 for more parametric details of the models.

4.2. Simulation

To simulate the data, we generate multiple 10-node graphs with 10×10 stable transition matrices. Using these we generate multivariate time series with autoregressive (VAR) and structural vector autoregressive (SVAR) models [44].

	Simulations	Real Data
Training Batch Size	16	min(32, no. of subjects)
Validation Batch Size	200	no. of subjects
Test Batch Size	200	no. of subjects
Initial Learning Rate	3e-4	3e-4
Learning Rate Scheduler	None	Reduce LR on Plateau
Max Epochs	500	3000

Table 1. Parameter details of models used for experiments

First, we generate 50 VAR times series with size 10×20000 . Then we split our dataset to $50 \times 10 \times 14000$ samples for training, $50 \times 10 \times 4000$ —for validation and $50 \times 10 \times 2000$ — for testing. Using these samples, We pre-train an encoder to learn consecutive windows (positive examples) from the same VAR time series. As mentioned in Section 3.1.2, we also use autoencoder for pre-training the same encoder and show the effectiveness of ST-DIM to learn time-series dynamics in self-supervised manner. After pre-training, we use our pre-trained encoder for complete-time series classification.

In the final downstream task, we classify the whole time-series whether it is generated by VAR or SVAR (undersampled VAR at rate 2). We create 400 graphs with corresponding stable transition matrices and generate $2000 \times 10 \times 4000$ samples (5 for each) and split as $1600 \times 10 \times 4000$ for training, $200 \times 10 \times 4000$ for validation and $200 \times 10 \times 4000$ for hold-out test. Here we also use 10×20 windows as a single time-point input.

First, we train our encoder to learn consecutive 10×20 windows from the VAR time series using InfoNCE based loss, and secondly, we train a supervised classifier based on windows. This window-based classification provides promising results. However, in solving similar real problems, we are more interested in subjects, i.e., entire time series, rather than a single-window for classification. Hence, we perform classification based on the whole time-series. In this setting, the entire time-series is encoded as a sequence of representations and fed through a biLSTM. Then, as described in Section 4.1, using the feed forward network on top of the last hidden state of the biLSTM, we map the representation to classification scores.

We observe that the ST-DIM based pre-trained models can easily be fine-tuned only with small amount of downstream data. In this classification task, our model can classify a randomly chosen time-series as a sample of VAR or SVAR. Note, with very few samples, models based on the pre-trained encoder (FPT and UFPT) outperform supervised models. However, as the number of samples grows, the accuracy achieved with or without pre-training levels out. We also notice that autoencoder based self-supervised pre-training does not assist in VAR vs. SVAR classification. Consequently, we use only ST-DIM based pre-training for all the real data experiments. Refer to Figure 4 for the results of simulation experiments.

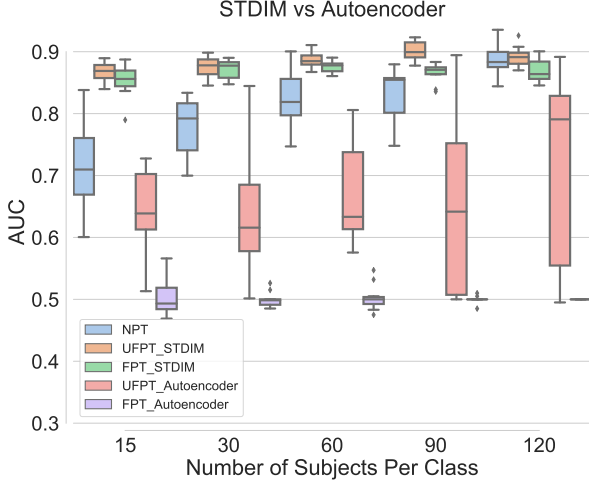


Figure 4. Area Under Curve (AUC) scores for VAR vs. SVAR time-series classification using ST-DIM and autoencoder based pre-training methods. ST-DIM based pre-training greatly improves the performance of downstream task with small datasets. On the other side, autoencoder based pre-training fails to learn dynamics and thus exhibits poor performance.

4.3. Keyword Detection

To show the broad implications of unsupervised pre-training, we first apply it to a simple problem of keyword detection in audio files. We choose this problem as it has many practical applications (e.g., virtual assistants in smart phones, robots). We use LibriSpeech ASR corpus [45] for pre-training and Speech Commands Dataset [46] for supervised training. The audio files of both datasets are combined with a background noise of coffee shop collected from [47] to make pre-training and classification harder.

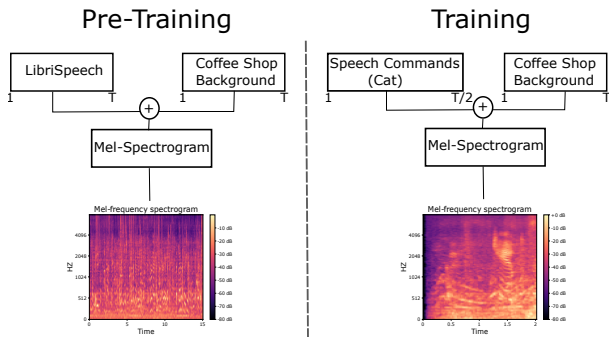


Figure 5. **Left:** For pre-training, we combine audio files from LibriSpeech dataset with background noise of coffee shop. T is the length of audio files which ranges from 1 to 20 seconds. **Right:** For training, we superimpose a $T/2$ length audio of word "cat" padded with $T/2$ zeros onto a background noise of coffee shop of length T ($T = 2$). For both pre-training and training, we calculate the mel-spectrogram of the combined audio files that results in a matrix of size *components* \times *time courses* for each audio file.

For pre-training, we calculate mel-spectrogram for all audio files from each subject and then concatenate together, resulting in a matrix of dimensions $C \times N$, where N , ranging anywhere from 10000 to 60000 depending on the length and number of audio files for each subject, is the time courses for the subject and $C = 128$ is the number of components in mel-spectrogram calculated at each time point. Figure 5 left shows the pre-processing of one audio file from a subject used for pre-training.

Out of all the available subjects, we select 416 which have large number of time points ($N \geq 20k$). We use 300 subjects for training and 116 for validation. For pre-training, we use the algorithm as described in section 3.1.1 and achieve accuracy of ~ 0.95 on the validation dataset.

For the downstream classification task, we collect samples of audios for the keyword "cat" from [46] which has 1515 audio files for the keyword. To create "cat" class examples, we superimpose each of the keyword audios having length of 1 second onto a 2 seconds long background noise at random location, resulting into a two seconds long audio consisting of background noise and keyword cat. Figure 5 Right shows the pre-processing used in downstream classification for a "cat" example. To create "no cat" class examples, we use another 1515, 2 seconds long audio files containing only background noise of coffee shop. Thus, we use 3030 audio files for the downstream task ("cat"/"no cat" classification). For all of the 3030 audio files, we compute mel-spectrogram to convert each of them into a matrix of size *components* \times *time courses*.

We perform 20 cross validations, each having a hold out of size 128 for test subjects. For each hold out, we conduct 5 different experiments varying number of samples (ranging from 15 to 100) from each class to be used for training. For each experiment, we perform 10 trials resulting into 200 trials to get accurate estimates of the performance.

As observed in the simulation experiments, Figure 6 shows the importance of ST-DIM based unsupervised pre-training for keyword detection problem. Even with very few training subjects, FPT and UFPT outperform NPT by a noticeable margin. As the number of samples increases, the performance of NPT improves but still remains much lower than the pre-trained counterparts.

4.4. Brain Imaging

4.4.1 Datasets

Next, we apply the same unsupervised pre-training method to brain imaging data. For encoder pre-training, we use HCP [5] consortium dataset and apply the pre-trained encoder for further downstream tasks. We apply the same pre-trained encoder for three different types of diseases spanning four datasets to classify schizophrenia, autism and Alzheimer's diseases. We use resting fMRI data for all brain

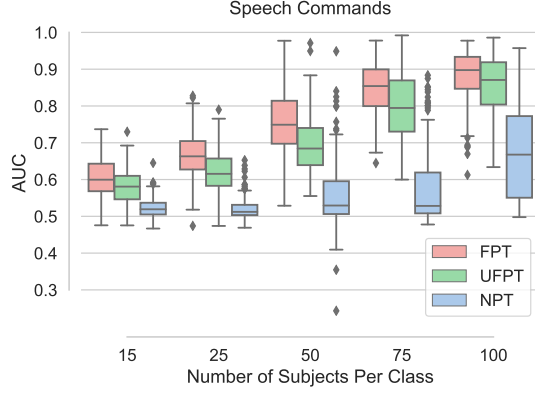


Figure 6. AUC scores for all the models on keyword detection task. Notice that pre-trained models provide noticeably better performance than NPT even with just 15 subjects for training. The pre-trained models continue to improve significantly reaching more than 0.9 with just 100 subjects, whereas NPT fails to achieve even 0.8 with the same number of training subjects.

data experiments. Refer to Figure 7 for the details of the datasets for disease classification.

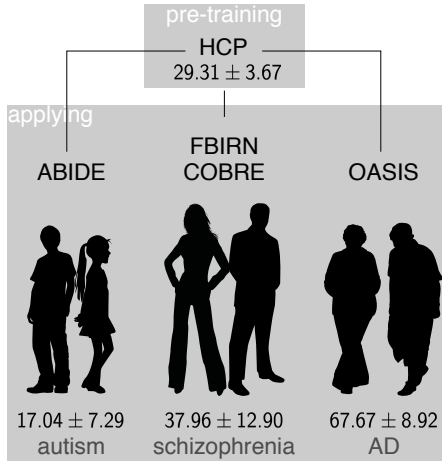


Figure 7. Datasets used for pre-training and classification tasks. Healthy controls from the HCP [5] are used for encoder pre-training guided by data dynamics alone¹. The pre-trained encoder is then used in downstream classification tasks of 3 different diseases, 4 independently collected datasets, many of which contain data from a number of sites, and consist of populations with significant age difference. The age distributions in the datasets have the following means, medians and standard deviations: **HCP**: 29.31, 29.00, 3.667; **ABIDE**: 17.04, 15.40, 7.29; **COBRE**: 37.96, 37, 12.90; **FBIRN**: 37.87, 38, 11.25; **OASIS**: 67.67, 68, 8.92.

Four datasets used in this study are collected from the FBIRN (Function Biomedical Informatics Research Network²) [48] project, from the COBRE (Center of Biomedical

¹Human silhouettes are by Natasha Sinagina for Creazilla.com without modifications, <https://creativecommons.org/licenses/by/4.0/>

²These data were downloaded from the Function BIRN Data Repository,

Research Excellence) [49] project, from the release 1.0 of ABIDE (Autism Brain Imaging Data Exchange³) [50] and from release 3.0 of OASIS (Open Access Series of Imaging Studies⁴) [51]. Written informed consent was obtained from all participants of each dataset under protocols approved by the institutional review board (IRB).

4.4.2 Preprocessing

We preprocessed the fMRI data using statistical parametric mapping (SPM12, <http://www.fil.ion.ucl.ac.uk/spm/>) under MATLAB 2016 environment. A rigid body motion correction was performed using the toolbox in SPM to correct subject head motion, followed by the slice-timing correction to account for timing difference in slice acquisition. The fMRI data were subsequently warped into the standard Montreal Neurological Institute (MNI) space using an echo planar imaging (EPI) template and were slightly resampled to $3 \times 3 \times 3 \text{ mm}^3$ isotropic voxels. The resampled fMRI images were finally smoothed using a Gaussian kernel with a full width at half maximum (FWHM) = 6 mm. After the preprocessing. We included subjects in the analysis if the subjects have head motion $\leq 3^\circ$ and $\leq 3 \text{ mm}$, and with functional data providing near full brain successful normalization [52].

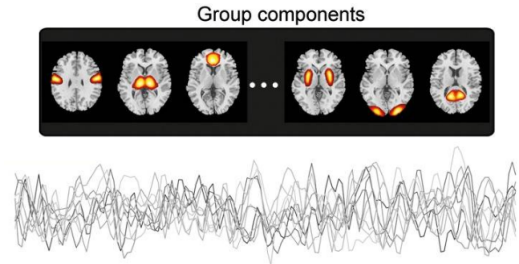


Figure 8. ICA time courses are computed from the resting state fMRI data. Results contain statistically independent spatial maps (top) and their corresponding time courses.

For each dataset, 100 ICA components as shown in Figure 8 are acquired using the same procedure described in [52]. However, only 53 non-noise components as determined per slice (time point) are used in pre-training of encoder and on downstream task. For experiments, including both pre-training and classification the fMRI sequence is divided into windows of 20 time points.

4.4.3 Schizophrenia

For schizophrenia classification, we conduct experiments on two different datasets, FBIRN [48] and COBRE [49]. The

Project Accession Number 2007-BDR-6UHZ1.

³http://fcon_1000.projects.nitrc.org/indi/abide/

⁴<https://www.oasis-brains.org/>

datasets contain labeled Schizophrenia (SZ) and Healthy Control (HC) subjects.

FBIRN The dataset has total 311 subjects consisting of 150 HC and 161 affected with SZ. Each subject has 53 non-noise components with 140 time points. We use two hold-out sets with sizes 32 and 64 respectively for validation and test. The remaining data are used for supervised training. With 140 time points, we create 53×20 -sized windows with 50% overlap along time dimension resulting in 13 windows for each subject. The details of the results are shown in Figure 9.

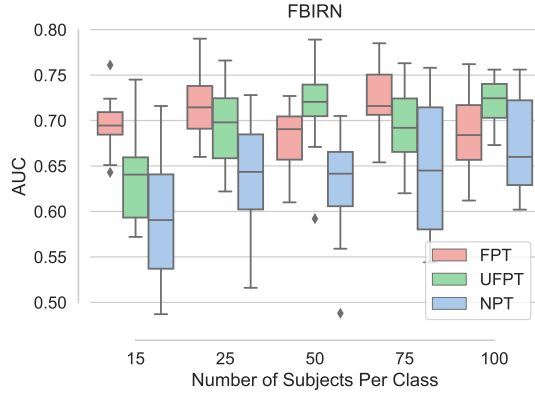


Figure 9. AUC scores for all the three models (Refer to Figure 3) on FBIRN dataset. It is noticeable that even with only 15 subjects for supervised training, the median AUC scores of FPT and NPT differ by a large margin (10%).

As we can see, the pre-trained models (FPT and UFPT) outperform NPT. Even with very few subjects (15) for training, the difference between AUC scores obtained respectively with FPT and NPT is reasonably large (≈ 0.1).

COBRE The dataset has total 157 subjects — a collection of 68 HC and 89 affected with SZ. Like FBIRN, each subject has 53 non-noise components in its ICA time courses with 140 time points. We use two hold-out sets of size 32 each respectively for validation and test. The remaining data are used for supervised training. With 140 time points, we create 53×20 -sized windows with no overlapping resulting in 7 windows for each subject. Unlike FBIRN, it has been impossible to increase the number of subjects for downstream training due to insufficiency of data.

The results in Figure 10 adheres to the results of FBIRN. That is, with only 15 training subjects, FPT and UFPT perform significantly better than NPT having ≈ 0.15 difference in their median AUC scores.

4.4.4 Autism

The dataset ABIDE has total 569 subjects, of which, 255 are HC and 314 are affected with autism. Like other datasets, each subject has 53 non-noise components with 140 time

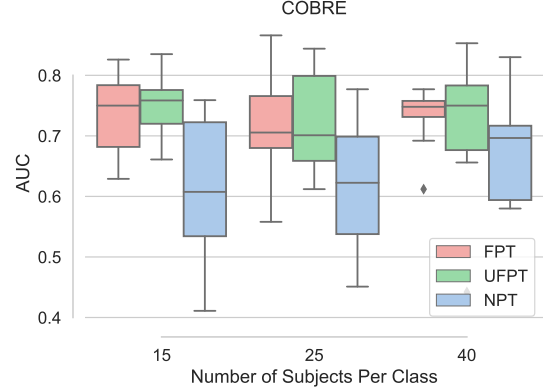


Figure 10. AUC scores for all the three models on COBRE dataset. It is obvious that even with 15 subjects for training, FPT outperforms NPT noticeably, that is, the difference between two median AUC scores is remarkable (≈ 0.15).

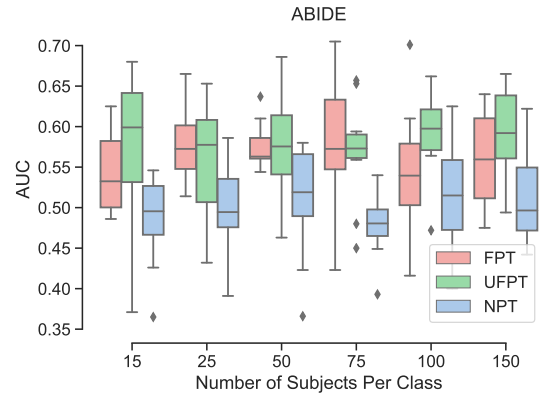


Figure 11. AUC scores for all the three models on ABIDE dataset. Like experiments on FBIRN and COBRE, it is evident that the pre-trained models consistently perform better than NPT.

points. We use two hold-out sets of size 100 each respectively for validation and test purpose. The remaining data are used for downstream training i.e., autism vs. HC classification. Like COBRE dataset, with 140 time points, we create 53×20 -sized windows with no overlapping resulting in 7 windows for each subject. Refer to Figure 11 for the details of the experimental results.

As seen in the figure, same pre-trained encoder performs reasonably better than NPT for autism vs. HC classification and thus reinforces our hypothesis that unsupervised pre-training learns signal dynamics useful for downstream tasks. Note the difference between age ranges of ABIDE and HCP datasets. The age range of ABIDE is much lower than that of HCP dataset used for pre-training. HCP dataset contains subjects of different ages with means 30.01 and 28.48, medians 30 and 28, and standard deviations 3.522 and 3.665 years respectively for female and male, whereas ABIDE dataset has overall mean 17.04, median 15.40 and standard deviation

7.29 years. Refer to Figure 7 for the demographic information of all the datasets. The dissimilarity in the age range is supposed to cause significant difference between these two datasets as the structure of brain and thought process of children is obviously different than adults.

4.4.5 Alzheimer’s disease

The dataset OASIS [51] has total 372 subjects with equal number (186) of HC and AZ patients. We use two hold-out sets each of size 64 respectively for validation and test purpose. The remaining are used for supervised training. Unlike other datasets described earlier, it has only 120 time points though the number of non-noise components is same (53) as other datasets. With 120 time points, we use six 53×20 -sized non-overlapping windows for each subject. Refer to Figure 12 for the details of the experiments.

As we see, the AUC scores of all the three models for 15 subjects is ~ 0.5 , which can be treated as merely random guess. However, as the number of subjects increases, pre-trained models gradually start performing better than NPT which, in fact, even with 120 subjects fails to learn from the data. We suspect that the reason why pre-trained models do not work for 15 subjects is that the data set is much different than HCP. The big age gap between subjects of HCP and OASIS is a major difference and 15 subjects are even not enough for pre-trained models.

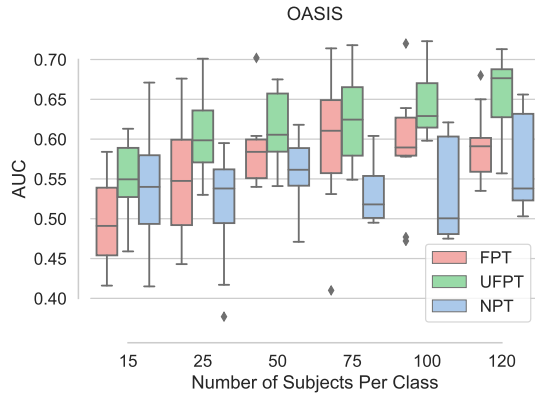


Figure 12. AUC scores for all the models on OASIS dataset. As we continue increasing the number of subjects, the pre-trained models start learning and thus improve their respective scores. However, notice that the NPT model even with 120 subjects didn’t significantly improve its predictability.

5. Conclusions and Future Work

As we have demonstrated, self-supervised pre-training of a spatiotemporal encoder gives significant improvement on the downstream tasks in both keyword detection and brain imaging datasets. Pre-training on fMRI of healthy

subjects provides benefits that transfer across datasets, collection sites, and multiple disease classification with varying age gap. Learning dynamics of fMRI helps to improve classification results for schizophrenia, autism, Alzheimer’s diseases and speed up the convergence of the algorithm on small datasets, that otherwise do not provide reliable generalizations. Although the utility of these results is highly promising by itself, we conjecture that direct application to spatio-temporal data will warrant benefits beyond improved classification accuracy in the future work. Working with ICA components is a smaller and thus easier to handle space that exhibits all dynamics of the signal, in future we will move beyond ICA pre-processing and work with fMRI data directly. We expect model introspection to yield insight into the spatio-temporal biomarkers of schizophrenia. In future work, we will use the same analogously pre-trained encoder on datasets with various other mental disorders such as MCI and bipolar. We are optimistic about the outcome because the proposed pre-training is oblivious of the downstream use and is done in a manner quite different from the classifier’s work. It may indeed be learning crucial information about dynamics that might contain important clues into the nature of mental disorders.

6. Acknowledgement

This study was supported by startup funds to SMP and in part by NIH grant R01EB020407.

Data for healthy subjects was provided [in part] by the Human Connectome Project, WU-Minn Consortium (Principal Investigators: David Van Essen and Kamil Ugurbil; 1U54MH091657) funded by the 16 NIH Institutes and Centers that support the NIH Blueprint for Neuroscience Research; and by the McDonnell Center for Systems Neuroscience at Washington University.

Data for Schizophrenia classification was used in this study were downloaded from the Function BIRN Data Repository (<http://bdr.birncommunity.org:8080/BDR/>), supported by grants to the Function BIRN (U24-RR021992) Testbed funded by the National Center for Research Resources at the National Institutes of Health, U.S.A. and from the Collaborative Informatics and Neuroimaging Suite Data Exchange tool (COINS; <http://coins.trendscenter.org>) and data collection was performed at the Mind Research Network, and funded by a Center of Biomedical Research Excellence (COBRE) grant 5P20RR021938/P20GM103472 from the NIH to Dr. Vince Calhoun.

Data for Alzheimer’s was provided by OASIS-3: Principal Investigators: T. Benzinger, D. Marcus, J. Morris; NIH P50AG00561, P30NS09857781, P01AG026276, P01AG003991, R01AG043434, UL1TR000448, R01EB009352. AV-45 doses were provided by Avid Radiopharmaceuticals, a wholly owned subsidiary of Eli Lilly.

Autism data was provided by ABIDE. We acknowledge primary support for the work by Adriana Di Martino provided by the (NIMH K23MH087770) and the Leon Levy Foundation and primary support for the work by Michael P. Milham and the INDI team was provided by gifts from Joseph P. Healy and the Stavros Niarchos Foundation to the Child Mind Institute, as well as by an NIMH award to MPM (NIMH R03MH096321).

References

- [1] David P Goldberg and Peter Huxley. *Common mental disorders: a bio-social model*. Tavistock/Routledge, 1992. 1
- [2] Vince D Calhoun, Robyn Miller, Godfrey Pearlson, and Tulay Adalı. The chroconnectome: time-varying connectivity networks as the next frontier in fmri data discovery. *Neuron*, 84(2):262–274, 2014. 1
- [3] Ali Khazaei, Ata Ebrahimzadeh, and Abbas Babajani-Feremi. Application of advanced machine learning methods on resting-state fMRI network for identification of mild cognitive impairment and Alzheimer’s disease. *Brain Imaging and Behavior*, 10(3):799–817, Sep 2016. 1
- [4] Weizheng Yan, Sergey Plis, Vince D Calhoun, Shengfeng Liu, Rongtao Jiang, Tian-Zi Jiang, and Jing Sui. Discriminating schizophrenia from normal controls using resting state functional network connectivity: A deep neural network and layer-wise relevance propagation method. In *2017 IEEE 27th International Workshop on Machine Learning for Signal Processing (MLSP)*, pages 1–6. IEEE, 2017. 1
- [5] David C Van Essen, Stephen M Smith, Deanna M Barch, Timothy EJ Behrens, Essa Yacoub, Kamil Ugurbil, Wu-Minn HCP Consortium, et al. The WU-Minn human connectome project: an overview. *Neuroimage*, 80:62–79, 2013. 1, 5, 6
- [6] Dumitru Erhan, Yoshua Bengio, Aaron Courville, Pierre-Antoine Manzagol, Pascal Vincent, and Samy Bengio. Why does unsupervised pre-training help deep learning? *Journal of Machine Learning Research*, 11(Feb):625–660, 2010. 2
- [7] Geoffrey E Hinton and Russ R Salakhutdinov. Using deep belief nets to learn covariance kernels for gaussian processes. In J. C. Platt, D. Koller, Y. Singer, and S. T. Roweis, editors, *Advances in Neural Information Processing Systems 20*, pages 1249–1256. Curran Associates, Inc., 2008. 2
- [8] Pascal Vincent, Hugo Larochelle, Yoshua Bengio, and Pierre-Antoine Manzagol. Extracting and composing robust features with denoising autoencoders. In *Proceedings of the 25th international conference on Machine learning*, pages 1096–1103. ACM, 2008. 2
- [9] Alex Krizhevsky, Ilya Sutskever, and Geoffrey E Hinton. Imagenet classification with deep convolutional neural networks. In *Advances in neural information processing systems*, pages 1097–1105, 2012. 2
- [10] Alec Radford, Jeffrey Wu, Rewon Child, David Luan, Dario Amodei, and Ilya Sutskever. Language models are unsupervised multitask learners. *OpenAI Blog*, 1(8), 2019. 2
- [11] Jacob Devlin, Ming-Wei Chang, Kenton Lee, and Kristina Toutanova. Bert: Pre-training of deep bidirectional transformers for language understanding. *arXiv preprint arXiv:1810.04805*, 2018. 2
- [12] Tomas Mikolov, Ilya Sutskever, Kai Chen, Greg S Corrado, and Jeff Dean. Distributed representations of words and phrases and their compositionality. In *Advances in neural information processing systems*, pages 3111–3119, 2013. 2
- [13] Jonas Gehring, Yajie Miao, Florian Metze, and Alex Waibel. Extracting deep bottleneck features using stacked auto-encoders. In *2013 IEEE international conference on acoustics, speech and signal processing*, pages 3377–3381. IEEE, 2013. 2
- [14] Dong Yu, Li Deng, and George Dahl. Roles of pre-training and fine-tuning in context-dependent dbn-hmms for real-world speech recognition. In *Proc. NIPS Workshop on Deep Learning and Unsupervised Feature Learning*, 2010. 2
- [15] Ian Goodfellow, Yoshua Bengio, and Aaron Courville. *Deep learning*. MIT press, 2016. 2, 3
- [16] Kaiming He, Ross Girshick, and Piotr Dollar. Rethinking imagenet pre-training. In *The IEEE International Conference on Computer Vision (ICCV)*, October 2019. 2
- [17] Aaron van den Oord, Yazhe Li, and Oriol Vinyals. Representation learning with contrastive predictive coding. *arXiv preprint arXiv:1807.03748*, 2018. 2
- [18] R Devon Hjelm, Alex Fedorov, Samuel Lavoie-Marchildon, Karan Grewal, Phil Bachman, Adam Trischler, and Yoshua Bengio. Learning deep representations by mutual information estimation and maximization. *arXiv preprint arXiv:1808.06670*, 2018.

- [19] Olivier J Hénaff, Ali Razavi, Carl Doersch, SM Eslami, and Aaron van den Oord. Data-efficient image recognition with contrastive predictive coding. *arXiv preprint arXiv:1905.09272*, 2019. 2
- [20] Philip Bachman, R Devon Hjelm, and William Buchwalter. Learning representations by maximizing mutual information across views. *arXiv preprint arXiv:1906.00910*, 2019.
- [21] Kaiming He, Haoqi Fan, Yuxin Wu, Saining Xie, and Ross Girshick. Momentum contrast for unsupervised visual representation learning, 2019. 2
- [22] Alex Fedorov, R Devon Hjelm, Anees Abrol, Zening Fu, Yuhui Du, Sergey Plis, and Vince D Calhoun. Prediction of progression to Alzheimers disease with deep InfoMax. *arXiv preprint arXiv:1904.10931*, 2019. 2
- [23] Ankesh Anand, Evan Racah, Sherjil Ozair, Yoshua Bengio, Marc-Alexandre Côté, and R Devon Hjelm. Unsupervised state representation learning in Atari. *arXiv preprint arXiv:1906.08226*, 2019. 2
- [24] Mirco Ravanelli and Yoshua Bengio. Learning speaker representations with mutual information. *arXiv preprint arXiv:1812.00271*, 2018. 2
- [25] J. Deng, W. Dong, R. Socher, L.-J. Li, K. Li, and L. Fei-Fei. ImageNet: A Large-Scale Hierarchical Image Database. In *CVPR09*, 2009. 2
- [26] Meenakshi Khosla, Keith Jamison, Gia H Ngo, Amy Kuceyeski, and Mert R Sabuncu. Machine learning in resting-state fMRI analysis. *Magnetic resonance imaging*, 2019. 2
- [27] Sergey M Plis, Devon Hjelm, Ruslan Salakhutdinov, Elena A Allen, Henry Jeremy Bockholt, Jeffrey D Long, Hans J Johnson, Jane Paulsen, Jessica A Turner, and Vince D Calhoun. Deep learning for neuroimaging: a validation study. *Frontiers in Neuroscience*, 8(229), 2014. 2
- [28] Vince D Calhoun, Tulay Adali, Godfrey D Pearlson, and JJ Pekar. A method for making group inferences from functional MRI data using independent component analysis. *Human brain mapping*, 14(3):140–151, 2001. 2
- [29] Harini Eavani, Theodore D Satterthwaite, Raquel E Gur, Ruben C Gur, and Christos Davatzikos. Unsupervised learning of functional network dynamics in resting state fmri. In *International Conference on Information Processing in Medical Imaging*, pages 426–437. Springer, 2013. 2
- [30] R Devon Hjelm, Vince D Calhoun, Ruslan Salakhutdinov, Elena A Allen, Tulay Adali, and Sergey M Plis. Restricted Boltzmann machines for neuroimaging: an application in identifying intrinsic networks. *NeuroImage*, 96:245–260, 2014. 2
- [31] R Devon Hjelm, Eswar Damaraju, Kyunghyun Cho, Helmut Laufs, Sergey M Plis, and Vince D Calhoun. Spatio-temporal dynamics of intrinsic networks in functional magnetic imaging data using recurrent neural networks. *Frontiers in neuroscience*, 12:600, 2018. 2
- [32] Meenakshi Khosla, Keith Jamison, Amy Kuceyeski, and Mert R Sabuncu. Detecting abnormalities in resting-state dynamics: An unsupervised learning approach. In *International Workshop on Machine Learning in Medical Imaging*, pages 301–309. Springer, 2019. 2
- [33] Arthur Mensch, Julien Mairal, Danilo Bzdok, Bertrand Thirion, and Gaël Varoquaux. Learning neural representations of human cognition across many fMRI studies. In *Advances in Neural Information Processing Systems*, pages 5883–5893, 2017. 2
- [34] Hailong Li, Nehal A. Parikh, and Lili He. A novel transfer learning approach to enhance deep neural network classification of brain functional connectomes. *Frontiers in Neuroscience*, 12:491, 2018.
- [35] Armin W Thomas, Klaus-Robert Müller, and Wojciech Samek. Deep transfer learning for whole-brain fMRI analyses. *arXiv preprint arXiv:1907.01953*, 2019. 2
- [36] Alvaro Ulloa, Sergey Plis, and Vince Calhoun. Improving classification rate of schizophrenia using a multimodal multi-layer perceptron model with structural and functional MR. *arXiv preprint arXiv:1804.04591*, 2018. 2
- [37] Aaron van den Oord, Yazhe Li, and Oriol Vinyals. Representation learning with contrastive predictive coding. *arXiv preprint arXiv:1807.03748*, 2018. 2
- [38] Michael Tschannen, Josip Djolonga, Paul K Rubenstein, Sylvain Gelly, and Mario Lucic. On mutual information maximization for representation learning. *arXiv preprint arXiv:1907.13625*, 2019. 2
- [39] Mark A Kramer. Nonlinear principal component analysis using autoassociative neural networks. *AICHE journal*, 37(2):233–243, 1991. 3
- [40] Mike Schuster and Kuldeep K Paliwal. Bidirectional recurrent neural networks. *IEEE Transactions on Signal Processing*, 45(11):2673–2681, 1997. 3

- [41] Xavier Glorot, Antoine Bordes, and Yoshua Bengio. Deep sparse rectifier neural networks. In *Proceedings of the fourteenth international conference on artificial intelligence and statistics*, pages 315–323, 2011. 3
- [42] Diederik P Kingma and Jimmy Ba. Adam: A method for stochastic optimization. *arXiv preprint arXiv:1412.6980*, 2014. 4
- [43] Xavier Glorot and Yoshua Bengio. Understanding the difficulty of training deep feedforward neural networks. In *Proceedings of the thirteenth international conference on artificial intelligence and statistics*, pages 249–256, 2010. 4
- [44] Helmut Lütkepohl. *New introduction to multiple time series analysis*. Springer Science & Business Media, 2005. 4
- [45] V. Panayotov, G. Chen, D. Povey, and S. Khudanpur. Librispeech: an ASR corpus based on public domain audio books. *ICASSP*, pages 5206–5210, 2015. 5
- [46] Pete Warden. Speech commands: A dataset for limited-vocabulary speech recognition. 2018. 5
- [47] Duff The Psych. One hour of hq coffee shop background noise. 2014. 5
- [48] David B Keator, Theo GM van Erp, Jessica A Turner, Gary H Glover, Bryon A Mueller, Thomas T Liu, James T Voyvodic, Jerod Rasmussen, Vince D Calhoun, Hyo Jong Lee, et al. The function biomedical informatics research network data repository. *Neuroimage*, 124:1074–1079, 2016. 6
- [49] Mustafa S Çetin, Fletcher Christensen, Christopher C Abbott, Julia M Stephen, Andrew R Mayer, José M Cañive, Juan R Bustillo, Godfrey D Pearlson, and Vince D Calhoun. Thalamus and posterior temporal lobe show greater inter-network connectivity at rest and across sensory paradigms in schizophrenia. *Neuroimage*, 97:117–126, 2014. 6
- [50] Adriana Di Martino, Chao-Gan Yan, Qingyang Li, Erin Denio, Francisco X Castellanos, Kaat Alaerts, Jeffrey S Anderson, Michal Assaf, Susan Y Bookheimer, Mirella Dapretto, et al. The autism brain imaging data exchange: towards a large-scale evaluation of the intrinsic brain architecture in autism. *Molecular psychiatry*, 19(6):659, 2014. 6
- [51] Eugene H Rubin, Martha Storandt, J Philip Miller, Dorothy A Kinscherf, Elizabeth A Grant, John C Morris, and Leonard Berg. A prospective study of cognitive function and onset of dementia in cognitively healthy elders. *Archives of neurology*, 55(3):395–401, 1998. 6, 8
- [52] Zening Fu, Arvind Caprihan, Jiayu Chen, Yuhui Du, John C Adair, Jing Sui, Gary A Rosenberg, and Vince D Calhoun. Altered static and dynamic functional network connectivity in alzheimer’s disease and subcortical ischemic vascular disease: shared and specific brain connectivity abnormalities. *Human Brain Mapping*, 2019. 6